



Studies of the Structural, Optical, Thermal, Electrical and Dielectric Properties of a Polyvinyl Alcohol/Sodium Alginate Blend Doped with Cu Nanoparticles and ZnO Nanorods as Hybrid Nanofillers for Use in Energy Storage Devices

Hassan G. El Gohary^{1,2} · Talal F. Qahtan³ · Huda G. Alharbi⁴ · G. M. Asnag⁵ · A. L. Waly⁶

Accepted: 30 January 2023 / Published online: 16 February 2023

© The Author(s), under exclusive licence to Springer Science+Business Media, LLC, part of Springer Nature 2023

Abstract

In this work, polyvinyl alcohol/sodium alginate (PVA/SA) blend was used as a polymeric material for fabricating nanocomposites reinforced with copper nanoparticles (Cu NPs) and zinc oxide nanorods (ZnO NRs) as hybrid nanofillers in different concentrations. The TEM micrographs show that the shape of Cu NPs is perfectly round spheres and the shape of ZnO NRs are rods. Both pure PVA/SA blend and nanocomposite samples were characterized using X-ray diffraction (XRD) and Fourier transform infrared (FTIR) analyses, which revealed presence of coordinated hydrogen bonds and highly amorphous PVA/SA blend structure. Moreover, as evidenced by the UV–Vis spectra, the presence of the hybrid nanofillers in the blend considerably enhanced its optical properties, as absorption was increased while the indirect energy gap was reduced from 4.82 eV for the pure blend to 1.93 eV for the sample with highest concentration. The inclusion of Cu NPs and ZnO NRs also enhanced the thermal stability at higher temperatures, as confirmed by the thermogravimetric (TGA) curves. In addition, the impedance spectroscopic study findings confirmed that the alternating current (AC) conductivity was enhanced by adding the nanofillers to the polymeric matrix. The DC conductivity value (σ_{dc}) of PVA/SA blend doped with 1.2 wt% of nanofiller was $3.16 \times 10^{-9} \text{ S.cm}^{-1}$, which increased by approximately three orders of magnitude due to the increase of charges carriers and the creation of 3-D channels that lead to an increase in the movement of charges carriers within the blend matrix. As the dielectric parameters, such as dielectric permittivity and electrical modulus, can be tuned by varying the nanofiller content, these nanocomposites can be utilized in the development of solid polymeric electrolytes for use in advanced high-density energy storage applications and flexible-microelectronic devices.

Keywords PVA · SA · Cu NPs · ZnO NRs · XRD · TGA · AC conductivity

✉ Talal F. Qahtan
t.qahtan@psau.edu.sa

✉ G. M. Asnag
g.asnag@yahoo.com

¹ Physics Department, Faculty of Science, Tanta University, Tanta 31527, Egypt

² Department of Physics, Faculty of Science & Arts, Qelwah, Al-Baha University, Al-Baha, Kingdom of Saudi Arabia

³ Physics Department, College of Science and Humanities in Al-Kharj, Prince Sattam Bin Abdulaziz University, Al-Kharj 11942, Saudi Arabia

⁴ Department of Physics, College of Science and Arts, Jouf University, Al-Qurayat Branch, P.O. Box 756, Sakaka, Saudi Arabia

⁵ Department of Optometry and Visual Science, College of Medical Sciences, Al-Razi University, Sana'a, Yemen

⁶ Basic Science Department, Higher Institute of Engineering and Technology, New Damietta, Egypt

Introduction

Polymer nanocomposites are obtained by dispersing nanosized materials (e.g., spheres, rods, plates) in a polymeric matrix for a variety of industrial applications [1, 2]. Academic and practitioner interest in these materials has grown in recent years due to their beneficial properties, such as greater reinforcement relative to conventionally doped polymers [3, 4]. Blending two or more polymers is an easy technique of produce and control of physical features within a synthetic system [2, 5].

Polymer blends have become more famous in the commerce and technology fields than the manufacturing homopolymers/copolymers in the last decades due to the blending that allowed the production of new materials with good features for the required applications at low-cost. These features mainly depend on the origin features of the blending component polymers [5, 6]. Extant research has primarily focused on polyvinyl alcohol (PVA) as a host material for nanofillers due to its good thermal stability, water solubility and chemical resistance, as well as optical transparency [6, 7]. PVA is also advantageous as it is non-toxic and non-carcinogenic, as well as bio-degradable and bio-compatible, and has the capacity to reduce to secondary alcohol groups [7, 8]. However, researchers have recently started to explore sodium alginate (SA) as an addition to PVA, as this natural, biodegradable, non-toxic, hydrophilic, biocompatible, water-soluble, anionic, and low-cost polymer [9, 10] possesses an amorphous structure and can be used to obtain a polymeric blend with superior characteristics compared to PVA [11]. The available experimental findings further indicate that, as the SA content increases, the phase separation in the sample will decrease due to the presence of hydroxyl groups in SA that react with PVA via hydrogen bonding. Thus far, SA has been employed in a variety of contexts, including paper production, medical applications, food packaging, and electrical devices [10, 12]. These applications can also benefit from materials that incorporate copper nanoparticles (Cu NPs) as they possess large specific area, good optical characteristics, high catalytic and antibacterial activity, and excellent thermal and chemical stability [13, 14]. Therefore, these nanoparticles can be utilized when designing materials used for producing super capacitors, as well as in sensing and catalytic hydrogenation processes [14, 15]. Moreover, nanoparticles exhibit features that differ from those of their bulk counterparts [15, 16]. Similar benefits can be attained from ZnO, as evident from its widespread application in optoelectronics both as a sensor and as a catalyst [17, 18]. To maximize its advantages, photocatalytic activity in particular, various physical and chemical methods have been used in extant studies to

synthesize different ZnO structures, such as nanorods, nanotubes, and nanospheres [18, 19]. Doping with ZnO has been shown to increase carrier mobility and photocatalysis efficiency, while the resulting materials are easy to fabricate and non-toxic, making them ideal for use in photovoltaic cells, semiconductors, and next-generation lithium-ion batteries [14, 19]. The literature survey depicts that the optical, thermal and electrical properties of the PVA/SA blend via the addition of hybrid nanofillers (Cu NPs and ZnO NRs) have not been observed yet and are so far to be found for increasing their industrial and technological uses. The structural differences and formations of the interactions between the polymeric matrix and the hybrid nanofillers are characterized using FT-IR, X-ray and TEM measurements. The optical and electrical features of the nanocomposites were examined, which can lead to the judgment of their effective uses in industries. Thus, the work reported in this paper aims to contribute to this research stream by examining the physical properties of PVA/SA blends incorporating different Cu nanoparticle (NP) and ZnO nanorod (NR) amounts intended for energy storage and optical device applications.

Materials

PVA (99% hydrolyzed, M.W. \approx 89 kg/mol) and copper NP powder were purchased from Sigma, Aldrich (USA), while SA powder (M.W. \approx 350 kg/mol) was purchased from LANXESS Co, zinc nitrate was procured from Merck, and sodium hydroxide was purchased from El Nasr Co. Egypt. In all preparations, double-distilled water (DDW) served as solvent.

ZnO NRs Synthesis

The zinc alkali solution required for the present study was obtained by dissolving 30 g of zinc nitrate and 8 g of sodium hydroxide in DDW after which the sodium hydroxide solution was heated to a specified temperature. Next, the zinc nitrate solution was slowly added into the sodium hydroxide under constant stirring. After allowing 90 min for reaction to develop, the resulting white precipitate collected at the bottom of a bottle was filtered and rinsed three times with DDW and ethanol, respectively. Finally, ZnO NRs were obtained by centrifugation and were left to dry in vacuum at 500 °C for three hours.

PVA/SA/Cu NPs – ZnO NRs Nanocomposite Synthesis

The PVA/SA blend (70:30 wt%) required to obtain the nanocomposite was synthesized by the standard casting method. For this purpose, PVA and SA were placed in a

solvent which was stirred for six hours to ensure complete dissolution. Next, different Cu NP and ZnO NR concentrations (0.00, 0.15, 0.30, 0.60 and 1.20 wt%, while ensuring 50:50 ratio) were sonicated in an aqueous solution for 10 min before gradually adding the contents to the PVA/SA blend. The obtained solution was stirred for eight hours, followed by tip sonication for eight minutes. Finally, the resulting homogenized PVA/SA/Cu NP–ZnO NR solutions were poured into Petri dishes and were left to dry completely at 45 °C.

Characterization of Prepared Samples

For the characterization of the polymeric samples containing different Cu NP and ZnO NR amounts, transmission electron microscopy (TEM) micrographs were taken by a JEM-2100 (JEOL) electron microscope. Moreover, a high-resolution X-ray diffraction (XRD) system (X'Pert/PRO Materials Research diffractometer PW-3040, PANalytical/Almelo, The Netherlands) was used to examine the crystalline structure, while Fourier transform infrared (FTIR) spectrometer (Spectrum GX/FTIR, Perkin/Elmer, Waltham, MA, U.S.A.) was employed to assess the absorption characteristics. In addition, UV–Vis spectra of the prepared samples were captured by a UV–Vis spectrophotometer (UV 1800 Shimadzu, Kyoto, Japan), while thermogravimetric (TGA) curves were obtained using the TGA apparatus (NETZSCH/STA/409CD, Germany, 5 °C/min scan rate, 0.01 °C/min accuracy) under nitrogen atmosphere to test the nanocomposite decomposition characteristics over a wide temperature range, i.e., from room temperature (RT) to 700 °C. The alternating current (AC) conductivity of prepared samples was investigated using an Agilent 4284a Precision LCR meter (Santa-Clara, CA, USA) in the frequency range spanning from 0.01 HZ to 2,000 kHz.

Results and Discussion

TEM Micrographs of Cu Nanoparticles and ZnO Nanorods

TEM was utilized to investigate the sizes, crystallinity, and shapes of the nanofillers used in the present study. As shown in Fig. 1a, most Cu NPs are perfectly rounded spheres with a diameter ranging from 6.10 to 20.91 nm, with an average of cca. 13.54 nm [20, 21]. On the other hand, Fig. 1b confirms that ZnO formed rods of 19.67–39.10 nm and 33.59–90.09 nm average width and length, respectively [22, 23]. These findings are confirmed by the corresponding XRD scans.

XRD Scans

The structure parameters and phase purity of Cu NPs and ZnO NRs were tested using XRD and the findings are shown in Fig. 2a. As can be seen from the graph, the spectrum pertaining to Cu NPs exhibits the strongest peak at $2\theta = 43.22^\circ$ which corresponds to the (111) plane, while the peak at $2\theta = 50.35^\circ$ is attributed to the (200) plane (JCPDS File Number 04–0836) [13, 16]. Both peaks are well-aligned with the reported values for the face centered cubic (FCC) metallic Cu, indicating that Cu NPs are free from any impurities. On the other hand, ZnO NRs produce spectra characterized by several peaks, located respectively at $2\theta = 31.67^\circ, 34.25^\circ, 36.11^\circ, 47.35^\circ, 56.34^\circ, 62.69^\circ,$ and 67.79° , which can be attributed to the (100), (002), (101), (102), (110), (311) and (312) planes (JCPDS, File Number 36–1451), confirming the crystalline structure of ZnO NRs [24, 25]. These findings are supported by the XRD pattern, confirming the single-phase nature and a hexagonal (wurtzite) structure of the ZnO NRs [24, 26]. The identified peaks were used to calculate the average crystallite size of Cu NPs and ZnO NRs using Scherer's relation [27]:

$$D = 0.94\lambda/B\cos\theta \quad (1)$$

where λ is the XRD wavelength, B denotes the line width at half maximum of the peak intensity, and θ represents the diffraction peak angle. These calculations yielded 14 and 31 nm average size for Cu NPs and ZnO NRs, respectively [28, 29]. Moreover, as can be seen from the XRD patterns generated by the pure PVA/SA blend and PVA/SA/Cu NPs–ZnO NRs nanocomposite samples provided in Fig. 2b, the PVA/SA blend produces a broad and diffused peak at around $2\theta = 19^\circ$, confirming its amorphous nature. However, addition of nanofillers increases the degree of amorphosity, while their random distribution increases the number of defects, thereby enhancing the electrical conductivity [18]. The addition of Cu NPs and ZnO NRs leads to further inter/intramolecular interactions that lead to softening chains backbones of the polymeric matrix and disruption of crystalline area [17, 18]. These structural differences within the nanocomposites denote that the PVA/SA structure is influenced by the presence of nanofillers. Therefore, films of the nanocomposites are expected to display an improvement in electrical conductivity [9, 17]. The XRD patterns produced by the PVA/SA/Cu NP–ZnO NR nanocomposite also incorporate the diffraction peaks at $2\theta = 31.67^\circ, 34.25^\circ, 36.11^\circ, 43.22^\circ, 47.35^\circ, 50.35^\circ, 56.34^\circ$ and 62.69° produced by pure nanofillers, confirming that their morphology has not been altered by inclusion into the PVA/SA blend [30, 31]. The crystallinity degree (Dc%) was obtained in term of size of crystalline (C) and amorphous (A) region: $Dc\% = C \times 100 / (C + A)$ [30]. The calculated Dc% values were reported in Table 1, where

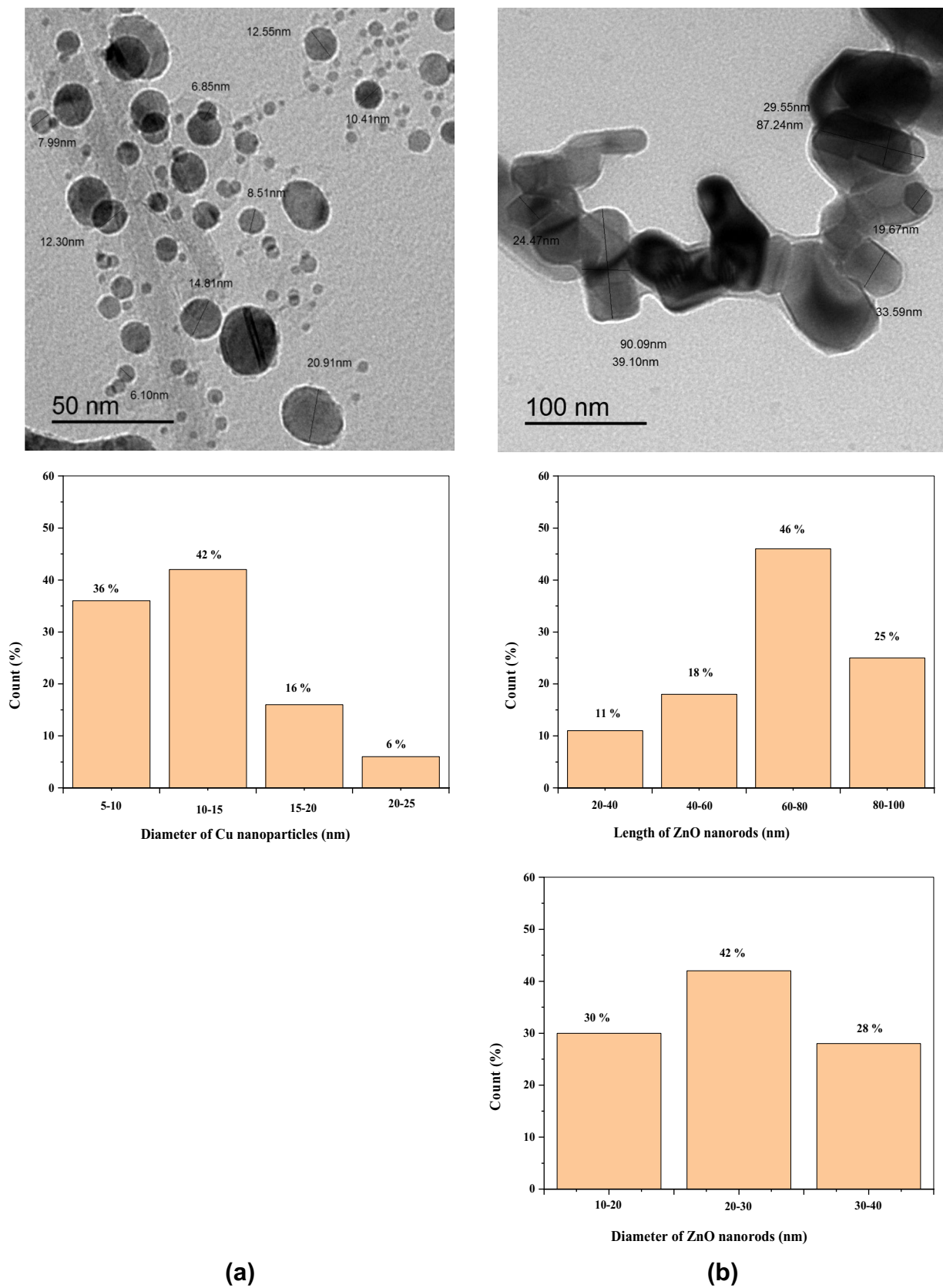


Fig. 1 The TEM micrographs and their histograms of: **a** Cu NPs and **b** ZnO NRs

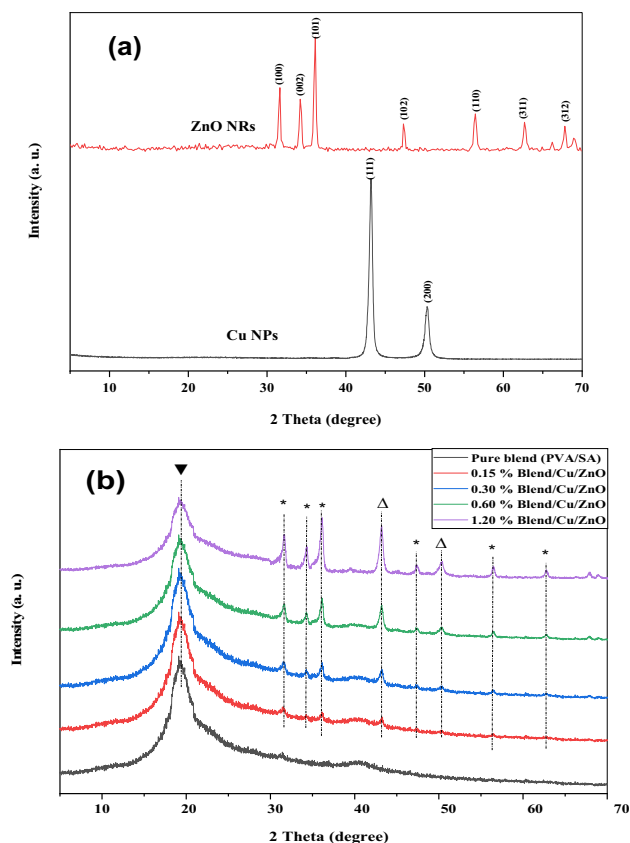


Fig. 2 The XRD scans of **a**: Cu NPs and ZnO NRs and **b**: PVA/SA/Cu NPs-ZnO NRs nanocomposite samples. *Note* The phase of PVA/SA blend was identified via the symbol (inverted triangle), while the phases of ZnO NRs and Cu NPs were identified via the symbols (*) and (triangle), respectively

the Dc % of the PVA/SA matrix decreased from 31.10% to 13.62% for the sample with the highest concentration of Cu NP–ZnO NR. These structural characteristics were further investigated through FTIR analysis.

FTIR Analysis

The PVA/SA pure blend and PVA/SA/Cu NP–ZnO NR nanocomposite samples were subjected to FTIR analysis to determine the interactions between the blend components

(PVA and SA) and the nanofillers, and the findings are shown in Fig. 3. Several peaks are evident in the FTIR spectrum produced by the pure PVA/SA blend, and that located at about 3330 cm^{-1} is attributed to OH stretching, while the peaks located at 2935 , 1724 and 1596 cm^{-1} can be ascribed to the asymmetric stretching vibration of CH_2 , stretching vibration in $\text{C}=\text{O}$ and COO^- stretching vibration, respectively [32–34]. Moreover, the bands at 1413 , 1318 and 1085 cm^{-1} are respectively attributed to bending vibrations in CH_2 , CH_2 wagging and $\text{C}-\text{O}$ stretching in the $\text{C}=\text{O}$ groups comprising the PVA backbone [34, 35]. On the other hand, the spectra produced by the PVA/SA/Cu NP–ZnO NR nanocomposite samples indicate that the presence of nanofillers reduced the absorption intensity without changing the position of the peaks for most of the functional groups, especially the bands of OH stretching, asymmetric stretching vibration of CH_2 , COO^- stretching vibration and COO^- stretching vibration, and this reduction is proportionate to the nanofiller concentration [36, 37, 39]. These findings reflect the interactions and structural arrangements between the blend and the nanofillers, such as the hydrogen and coordination bonding or Vander-Waals forces which increase the degree of amorphosity [38], that induced the presence of charges transfer complexes dominant between the hybrid nanoparticles and the polymeric chains and lowering in the degree of crystallinity as concurred in the XRD scans.

UV–Vis Analysis

Figure 4 displays the UV–Vis spectra produced by pure PVA/SA blend and PVA/SA/Cu NP–ZnO NR nanocomposite samples. The spectrum related to the pure PVA/SA blend displays an absorption peak at 210 nm which was attributed to the $\pi \rightarrow \pi^*$ electronic transitions due to the existence of the $\text{C}=\text{O}$ group within the polymer structure [39, 40]. This peak exhibits a red shift as well as an increase in amplitude as a result of addition of nanofillers in progressively greater concentrations. These changes suggest that the crystallinity ratio decreases as a result of the interactions and complexation between the polymeric chains and the Cu NPs and ZnO NRs, as showed in Table 1. In addition, the UV–Vis spectra

Table 1 The values of indirect, direct energy gaps, DC conductivity (σ_{dc}) and the crystallinity degree (Dc%) for PVA/SA/Cu NPs-ZnO NRs films

Samples	Dc%	σ_{dc} (S.cm ⁻¹)	E _g (eV)	
			Indirect E _g	Direct E _g
Pure sample	31.10	1.93×10^{-12}	4.82	5.26
Blend/0.15 wt% Cu NPs- ZnO NRs	26.85	2.75×10^{-10}	4.35	4.90
Blend/0.30 wt% Cu NPs- ZnO NRs	21.91	5.62×10^{-10}	2.45	3.51
Blend/0.60wt% Cu NPs- ZnO NRs	17.85	9.77×10^{-10}	2.14	3.24
Blend/1.20 wt% Cu NPs- ZnO NRs	13.62	3.16×10^{-9}	1.93	2.96

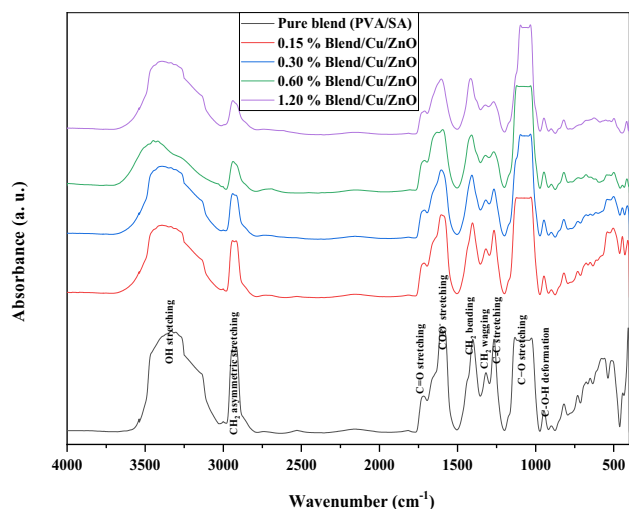


Fig. 3 FT-IR of PVA/SA samples doped with different ratios of Cu NPs and ZnO NRs

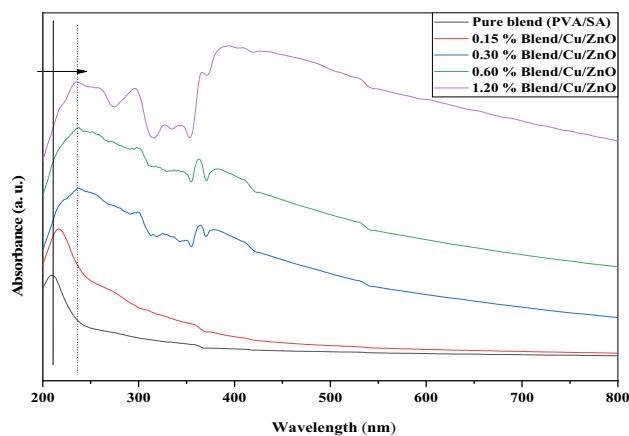


Fig. 4 The UV-Vis of PVA/SA samples doped with different ratios of Cu NPs-ZnO NRs

of doped films also incorporate a new band at about 379 nm which is produced by the electrons in ZnO NRs transitioning from the valance to the conduction band, giving rise to surface plasmon resonance (SPR) [41]. As the nanofiller concentration increases, the SPR peak increases in intensity and its position shifts to longer wavelengths, suggesting that the NR diameter has increased. This red shift also confirms the influence of quantum confinement. To further examine these optical phenomena, the optical energy gap (E_g) was determined by applying the following expression [42]:

$$\alpha h\nu = A(h\nu - E_g)^n \quad (2)$$

where $h\nu$ represents photon energy, A is a constant and n takes the value of 2 and 1/2 for allowed indirect and direct transitions, respectively. In the graphs shown in Figs. 5a and b, $(\alpha h\nu)^{1/2}$ and $(\alpha h\nu)^2$ is plotted as a function of photon energy ($h\nu$) of PVA/SA/Cu NP-ZnO NR samples. Moreover, the indirect and direct E_g values listed in Table 1 indicate that the E_g values of pure PVA/SA blend are in good agreement with those reported in the literature (4.82 and 5.26 eV for indirect and direct E_g , respectively) [39, 41]. It is also evident from Table 1 that both indirect and direct E_g of doped samples decrease with the increase in nanofiller content due to the greater defect production as well as greater disorder ratio, as new energy levels are generated by the inclusion of Cu NPs and ZnO NRs [41, 42].

TGA Analysis

As can be seen from the TGA scans of PVA/SA/Cu NP-ZnO NR nanocomposite samples shown in Fig. 6, TGA results in weight loss, due to evaporation of absorbed moisture below 100 °C, mass loss within the 225–300 °C

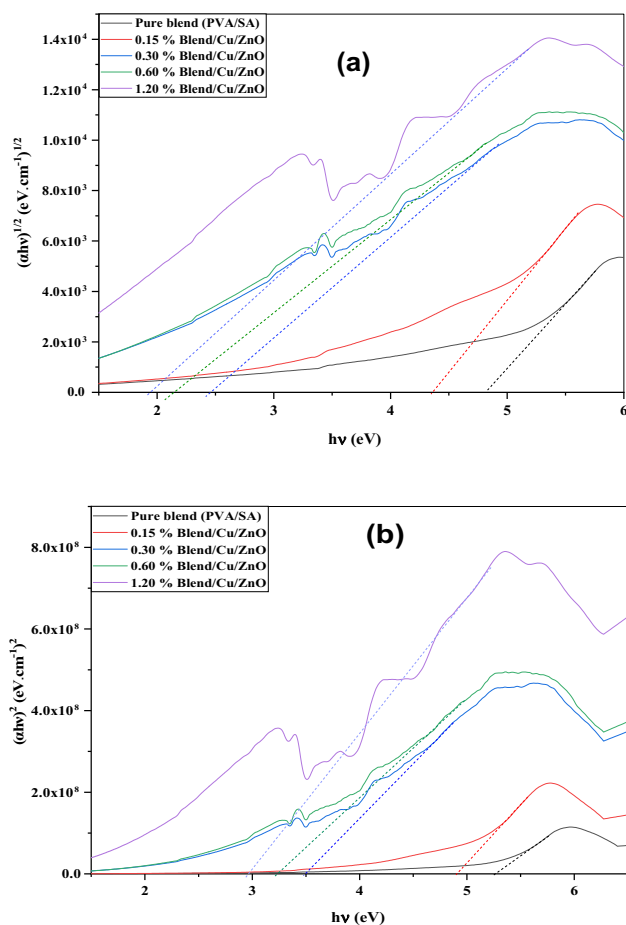


Fig. 5 a: $(\alpha h\nu)^{1/2}$ and b: $(\alpha h\nu)^2$ versus photon energy plots of PVA/SA samples doped with different ratios of Cu NPs-ZnO NRs

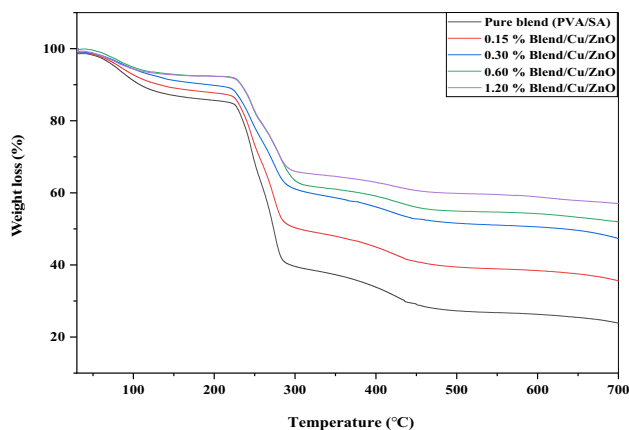


Fig. 6 TGA curves of PVA/SA samples doped with different ratios of Cu NPs and ZnO NRs

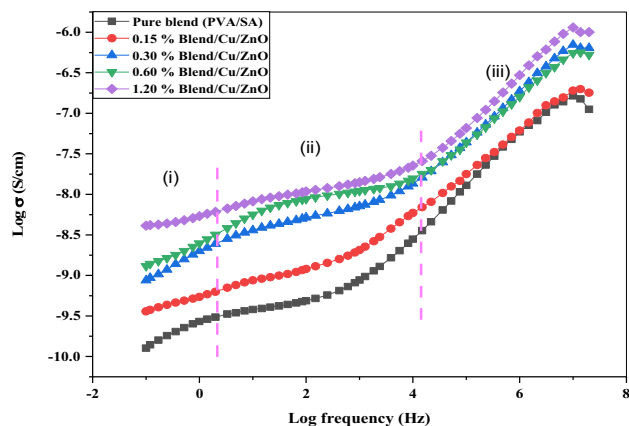


Fig. 7 Plots of $\log \sigma$ versus \log frequency of PVA/SA samples doped with different ratios of Cu NPs and ZnO NRs

range (due to the loss of OH groups such as H_2O , aldehydes, and methyl ketone) [43] and the decomposition products (carbon and hydrocarbons, generated by the degradation of blend structure) at about $438^\circ C$ [43, 44]. On the other hand, nanofiller addition reduces the weight loss and thus improves thermal stability. These findings are expected, as the flexibility and softening of blend chains are reduced by the inclusion of Cu NPs and ZnO NRs, allowing for strong cross-linking interactions between the polymeric molecules and the nanofillers. This enhancement can be ascribed to the homogeneous dispersion of Cu NPs and ZnO NRs within the PVA/SA blend, allowing the nanofillers to efficiently inhibit the polymeric structure degradation [43, 45].

AC Conductivity

Figure 7 shows the variation in (σ_{ac}) conductivity as a function of nanofiller content [46] and frequency, which is governed by the Jonscher's power law given below [31]:

$$\sigma_{ac} = 1/\rho \quad (3)$$

where ρ is the electrical resistivity.

The increase in AC conductivity with a progressively greater nanofiller content is due to the increased charge carrier mobility as well as greater number of defects, in accordance with the percolation theory [46, 47]. Specifically, as the nanofiller content increases, the molecules begin to bridge the gap between two localized states, and having energy greater than the potential barriers between them facilitates charge carrier transport [7]. From the Figure, the conductivity shows three distinct parts: (i) the lower frequencies dispersion part, (ii) the frequency-independent plateau part and (iii) the higher frequencies scattering region. The lower values of conductivity in the lower frequencies dispersion part (i) was due to the accumulation of ions (electrodes-polarization), which results from the slow periodic reversal of electrical fields [48, 49]. At the second part (ii), the middle part of frequencies denotes to the frequency independent plateau part and the DC conductivity can be calculated from this part. The high-frequency scattering part is assigned to the space charges polarization at the blocking electrodes. These scattering parts obey the Jonscher's power law equation [50, 51]. Table 1 shows the measured DC conductivity values at ambient temperature. As showed in the Table, the DC conductivity of the polymeric matrix increased to $3.16 \times 10^{-9} S.cm^{-1}$ for the PVA/SA blend doped with 1.2 wt.% of the hybrid nanoparticles. Moreover, the raise of the DC conductivity detects that the Cu NPs and ZnO NRs produce a 3-D conductive channels in the nanocomposites [47, 51]. It is depicted that the added of the hybrid nanoparticles within the PVA/SA blend may have increased the favorable positions and produced some additional charges carriers [46].

Dielectric and Modulus Parameters

As shown in Figs. 8a and b depicting dielectric constant (ϵ') and dielectric loss (ϵ'') as a function of frequency, presence of Cu NPs and ZnO NRs results in a considerable involvement of the Maxwell Wagner Silars (MWS) mechanism of interfacial polarization (IP) due to the difference in the permittivity and conductivity between the nanofillers and the host blend [46, 47]. Moreover, ϵ' declines as the frequency increases from 10 to 30 kHz, as the dipoles cannot rotate in the direction of the externally applied field at higher frequencies [52]. In addition, as Cu NPs and ZnO NRs have higher

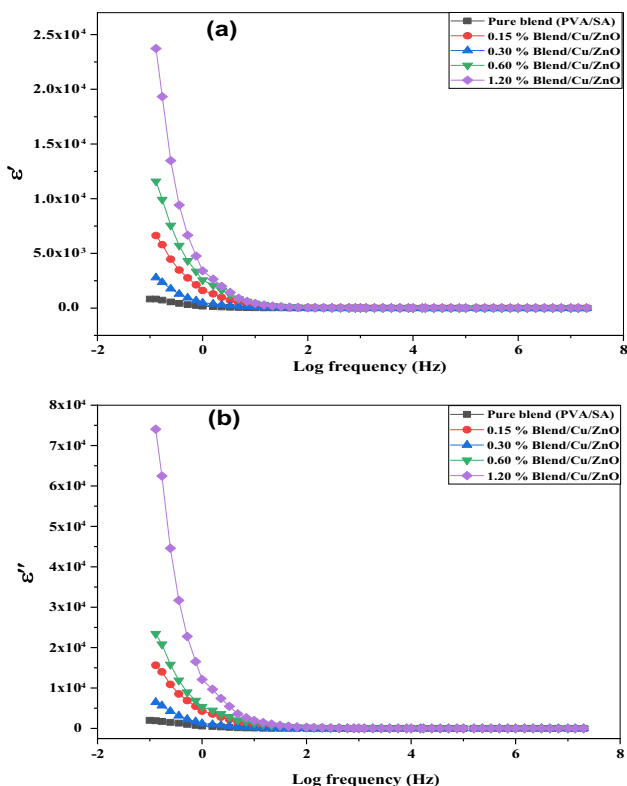


Fig. 8 Plots of **a**: ϵ' and **b**: ϵ'' versus log frequency of PVA/SA samples doped with different ratios of Cu NPs and ZnO NRs

ϵ' value than the pure blend; this increases the ϵ' value of the nanocomposites as a result of electrostatic interactions between the nanofillers and dipole groups in the polymeric matrix. This in turn assists in the correct dipole arrangement within the nanocomposite material, increasing its dielectric permittivity [52, 53]. Similarly, increase in nanofiller concentration increases the ϵ'' value due to the greater charge carrying capacity [7]. Similar trend is observed for the increase in frequency, which is attributed to greater charge mobility and thus to a decrease in polarization. The linear variation of the complex dielectric permittivity (ϵ' and ϵ'') values across the audio frequency range (below 20 kHz) confirms the dielectric behavior of nanocomposites, indicating that these materials can be used for producing nanoelectrodes for a variety of electronic applications [51, 53]. According to the available findings, these phenomena are expected, as nanofiller inclusion increases ionic conductivity, whereby the polymer chains become more flexible [7, 53].

Electric modulus of pure PVA/SA blend and PVA/SA/Cu NP – ZnO NR nanocomposite samples was also investigated as it reflects the relaxation process within heterogeneous structures. The real (M') and imaginary (M'') part versus frequency plots for pure PVA/SA blend and PVA/SA/Cu NP – ZnO NR nanocomposite samples are shown in

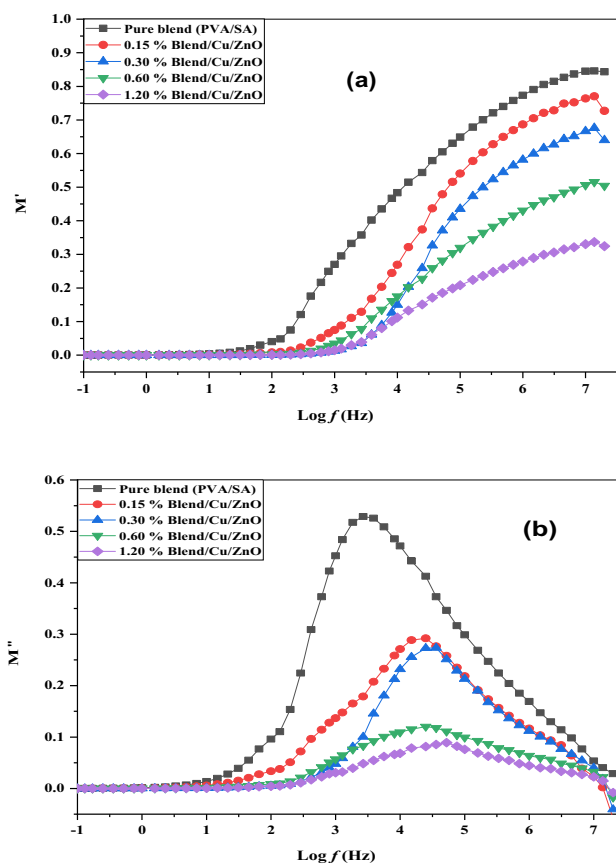


Fig. 9 Plots of **a**: M' and **b**: M'' versus log frequency of PVA/SA samples doped with different ratios of Cu NPs and ZnO NRs

Figs. 9a and b, respectively, and were obtained by applying the following calculations [54]:

$$M^* = 1/(\epsilon^*) = M' + iM'' \tag{4}$$

$$M' = \epsilon / (\epsilon'^2 + \epsilon''^2) \tag{5}$$

$$M'' = \epsilon'' / (\epsilon'^2 + \epsilon''^2) \tag{6}$$

As can be seen from Figs. 9a and b, the plots produced by both pure PVA/SA blend and PVA/SA/Cu NP – ZnO NR nanocomposite samples exhibit ‘step-like’ change in M' value, while the M'' values reflect the influence of MWS dynamics within the polymeric structure [53, 54], as the relaxation peaks shift upwards with the increase in frequency and the nanofiller amount within the polymeric matrix. Moreover, M' values are the lowest at the lowest frequency due to the negligible effect of electrode polarization [54, 55], while the M'' curves confirm that the addition of nanofillers promotes relaxation. It also reduces the strength of hydrogen bonds within the blend,

as the modulus relaxation time (τ_M) is a function of f_M — $\tau_M = 1/2\pi(f_M)$ —where f_M is the frequency of relaxation peaks [56]. Furthermore, these shifts in peak positions confirm the previous observation that the Cu NP and ZnO NR inclusion enhances charge carrier mobility by building conductive paths in the PVA/SA blend [55, 56].

Conclusion

PVA/SA blend electrolyte was prepared via doping with different concentrations of Cu NPs/ZnO NRs and was prepared using solution casting method. The increase in the amorphous degree of the doped samples was confirmed by XRD scans. The FTIR spectra showed the complexity and the strong interactions between the hybrid nanofillers and functional groups of the blend. Moreover, the UV–visible spectra revealed that the optical absorption was significantly increased due to the inclusion of the hybrid nanoparticles, while the optical energy gap was reduced due to the presence of charge transfer complexes. TGA scans of the nanocomposite films confirmed that the interactions between the polymer blend and the Cu NPs and ZnO NRs (which inhibit the degradation of the blend bonds) enhanced the thermal stability of the nanocomposites. The complex dielectric permittivity and electrical modulus spectra of these samples confirmed, at first, that ϵ' and ϵ'' decrease gradually with increasing frequency, but remain constant at higher frequencies. On the other hand, the M'' peak intensity increases and its position shift toward higher frequencies with the increase in the nanofiller content. The maximum value of AC conductivity has been found to be $1.23 \times 10^{-6} \text{ S}\cdot\text{cm}^{-1}$ at ambient temperature for PVA/SA blend doped with 1.2 wt% of the hybrid nanoparticles. These beneficial findings indicate that Cu NPs and ZnO NRs improve the dielectric and structural properties, as well as thermal and electrical conductivity of the PVA/SA blend, making this nanocomposite suitable for a variety of applications. This confirms the potential candidates as tunable nano-electrochemical and ionic conducting samples for biodegradable microelectronic applications such as organic electronic sensors, high-density energy storage, harvesting devices, high dielectric constant layers in transistors and the development of solid electrolytes polymeric materials.

Author Contribution HGEG: Funding acquisition, Project administration, Data curation. TFQ: Supervision, Software, Validation, Visualization. HGA: Conceptualization, Investigation. GMA: Supervision, Formal analysis, Resources, Writing – original draft. ALW: Methodology, Writing – review and editing.

Funding This study is supported via funding from Prince Sattam Bin Abdulaziz University, project number (PSAU/2023/R/1444).

Declarations

Conflict of interest The authors declare no conflict of interest.

References

- Sai T, Ran S, Guo Z, Song P, Fang Z (2022) Recent advances in fire-retardant carbon-based polymeric nanocomposites through fighting free radicals. *SusMat* 2:411–434
- Morsi MA, Abdelrazek EM, Ramadan RM, Elashmawi IS, Rajeh A (2022) Structural, optical, mechanical, and dielectric properties studies of carboxymethyl cellulose/polyacrylamide/lithium titanate nanocomposites films as an application in energy storage devices. *Polym Test* 114:107705
- Pirsaheb M, Gholami T, Seifi H, Yousif QA, Niasari MS (2022) Investigate of electrochemical hydrogen storage and coulombic efficiency of NiAl₂O₄/NiO synthesized by cationic, anionic and polymeric surfactants: green synthesis and characterization. *Int J Hydrog Energy* 47:34994–35002
- Ruan QD, Liu LL, Wu DH, Feng JJ, Zhang L, Wang AJ (2022) Cobalt phosphide nanoparticles encapsulated in manganese, nitrogen co-doped porous carbon nanosheets with rich nanoholes for high-efficiency oxygen reduction reaction. *J Colloid Interface Sci* 627:630–639
- Heiba ZK, Mohamed MB, Ahmed SI (2022) Exploring the physical properties of PVA/PEG polymeric material upon doping with nano gadolinium oxide. *Alex Eng J* 61:3375–3383
- Morsi MA, Asnag GM, Rajeh A, Awwad NS (2021) Nd:YAG nanosecond laser induced growth of Au nanoparticles within CMC/PVA matrix: multifunctional nanocomposites with tunable optical and electrical properties. *Compos Commun* 24:100662
- Atta MR, Alsulami QA, Asnag GM, Rajeh A (2021) Enhanced optical, morphological, dielectric, and conductivity properties of gold nanoparticles doped with PVA/CMC blend as an application in organoelectronic devices. *J Mater Sci Mater Electron* 32:10443–10457. <https://doi.org/10.1007/s10854-021-05701-3>
- Awwad NS, El-Kader MFHA, Ibrahim HA, Asnag GM, Morsi MA (2021) Green synthesis of different ratios from bimetallic gold: Silver nanoparticles core@shell via laser ablation scattered in Chitosan-PVA matrix and its electrical conductivity behavior. *Compos Commun* 24:100678
- Alshehari AM, Salim E, Oraby AH (2021) Structural, optical, morphological and mechanical studies of polyethylene oxide/sodium alginate blend containing multi-walled carbon nanotubes. *J Mater Res Technol* 15:5615–5622
- Zhang G, Chen HY, Yang G, Fu H (2022) Preparation of in situ ZIF-9 grown on sodium alginate/polyvinyl alcohol hydrogels for enhancing Cu (II) adsorption from aqueous solutions. *J Inorg Organomet Polym Mater* 32:4576–4588. <https://doi.org/10.1007/s10904-022-02463-1>
- Shetty GR, Rao BL (2022) Preparation and characterization of silk fibroin-polyvinyl alcohol (PVA) blend films for food packaging materials. *Mater Today: Proc* 55:194–200
- Ali M, Oshiki M, Rathnayake L, Ishii S, Satoh H, Okabe S (2015) Rapid and successful start-up of anammox process by immobilizing the minimal quantity of biomass in PVA-SA gel beads. *Water Res* 79:147–157
- Sardar S, Maity S, Pal S, Parvej H, Das N, Sepay N, Sarkar M, Halder UC (2016) Facile synthesis and characterization of beta

- lactoglobulin–copper nanocomposites having antibacterial applications. *RSC Adv* 6:85340–85346
14. Yuan S, Shen F, Chua CK, Zhou K (2019) Polymeric composites for powder-based additive manufacturing: materials and applications. *Prog Polym Sci* 91:141–168
 15. Abdallah EM, Qahtan TF, Abdelrazek EM, Asnag GM, Morsi MA (2022) Enhanced the structural, optical, electrical and magnetic properties of PEO/CMC blend filled with copper nanoparticles for energy storage and magneto-optical devices. *Opt Mater* 134:113092
 16. Reznickova A, Orendac M, Kolska Z, Cizmar E, Dendisova M, Svorcik V (2016) Copper nanoparticles functionalized PE: preparation, characterization and magnetic properties. *Appl Surf Sci* 390:728–734
 17. Abutalib MM (2019) Effect of zinc oxide nanorods on the structural, thermal, dielectric and electrical properties of polyvinyl alcohol/carboxymethyl cellulose composites. *Phys B Condens* 557:108–116
 18. Dhatarwa P, Sengwa RJ (2021) Nanofiller controllable optical parameters and improved thermal properties of (PVP/PEO)/Al₂O₃ and (PVP/PEO)/SiO₂ nanocomposites. *Optik* 233:166594
 19. Tarabiah AE, Alhadlaq HA, Alaizeri ZA, Ahmed AAA, Asnag GM, Ahamed M (2022) Enhanced structural, optical, electrical properties and antibacterial activity of PEO/CMC doped ZnO nanorods for energy storage and food packaging applications. *J Polym Res* 29:1–16. <https://doi.org/10.1007/s10965-022-03011-8>
 20. Elsayed A, Li W, El-Kady OA, Daoush WM, Olevsky EA, German RM (2015) Experimental investigations on the synthesis of W-Cu nanocomposite through spark plasma sintering. *J Alloys Compd* 639:373–380
 21. Song G, Han L, Zou W, Xiao Z, Huang XJ, Qin Z, Zou R, Hu J (2014) A novel photothermal nanocrystals of Cu₇S₄ hollow structure for efficient ablation of cancer cells. *Nanomicro Lett* 6(2):169–177. <https://doi.org/10.1007/BF03353781>
 22. Asnag GM, Awwad NS, Ibrahim HA, Moustapha ME, Alqahtani MS, Menazea AA (2022) One-pot pulsed laser ablation route assisted molybdenum trioxide nano-belts doped in PVA/CMC blend for the optical and electrical properties enhancement. *J Inorg Organomet Polym Mater* 32:2056–2064. <https://doi.org/10.1007/s10904-022-02257-5>
 23. Padilla CKZ, Sandoval JG, Gamboa SA (2022) A feasible and low-cost green route to prepare ZnO with n or p-type conductivity by changing the parsley extract concentration. *J Alloys Compd* 891:162087
 24. Dhole SG, Dake SA, Prajapati TA, Helambe SN (2018) Effect of ZnO filler on structural and optical properties of polyaniline-ZnO nanocomposites. *Procedia Manuf* 20:127–134
 25. Qiao F, Sun K, Liu W, Xie Y, Chu H (2022) Bandgap modulation of ZnO/ZnS heterostructures through ion exchange and their efficient transport properties. *Vacuum* 196:110788
 26. Karpuraranjith M, Thambidurai S (2017) Chitosan/zinc oxide-polyvinylpyrrolidone (CS/ZnO-PVP) nanocomposite for better thermal and antibacterial activity. *Int J Biol Macromol* 104:1753–1761
 27. Sebak MA, Qahtan TF, Asnag GM, Abdallah EM (2022) The Role of TiO₂ nanoparticles in the structural, thermal and electrical properties and antibacterial activity of PEO/PVP blend for energy storage and antimicrobial application. *J Inorg Organomet Polym Mater* 32:4715–4728
 28. Morsi MA, Abdelaziz M, Oraby AH, Mokhles I (2019) Structural, optical, thermal, and dielectric properties of polyethylene oxide/carboxymethyl cellulose blend filled with barium titanate. *J Phys Chem Solids* 125:103–114
 29. Morsi MA, Rajeh A, Al-Muntaser AA (2019) Reinforcement of the optical, thermal and electrical properties of PEO based on MWCNTs/Au hybrid fillers: nanodielectric materials for organo-electronic devices. *Compos B Eng* 173:106957
 30. Atta MR, Algethami N, Farea MO, Alsulami QA, Rajeh A (2022) Enhancing the structural, thermal, and dielectric properties of the polymer nanocomposites based on polymer blend and barium titanate nanoparticles for application in energy storage. *Int J Energy Res* 46:8020–8029
 31. Abdallah EM, Morsi MA, Asnag GM, Tarabiah AE (2022) Structural, optical, thermal, and dielectric properties of carboxymethyl cellulose/sodium alginate blend/lithium titanium oxide nanoparticles: Biocomposites for lithium-ion batteries applications. *Int J Energy Res* 46:1–17
 32. Kumar R, Kumar R, Sharma PK, Sharma A (2022) Synthesis and characterization of PVA embedded with peanut-shaped Ag₂Ag nanoparticles: optical and electrical properties. *Polym Bull.* <https://doi.org/10.1007/s00289-022-04396-8>
 33. Zidan HM, Abdelrazek EM, Abdelghany AM, Tarabiah AE (2019) Characterization and some physical studies of PVA/PVP filled with MWCNTs. *J Mater Res Technol* 8:904–913
 34. Omkaram I, Chakradhar RS, Rao JL (2007) EPR, optical, infrared and Raman studies of VO²⁺ ions in polyvinylalcohol films. *Phys B Condens* 388:318–325
 35. Zhou Y, Chai Y, Miyata M, Tagaya M (2022) Preparation of citric acid-modified poly (vinyl alcohol) films for effectively precipitating calcium phosphate particles. *CrystEngComm* 24:5552–5556
 36. Xu Y, Li J, Li W (2022) Evolution in electrochemical performance of the solid blend polymer electrolyte (PEO/PVDF) with the content of ZnO nanofiller. *Colloids Surf Physicochem Eng Asp* 632:127773
 37. Sengwa RJ, Patel VK, Saraswat M (2022) Investigation on promising properties of PEO/PVP/LiTFSI solid polymer electrolytes for high-performance energy storage and next-generation flexible optoelectronic and iontronic devices. *J Polym Res* 29:1–22. <https://doi.org/10.1007/s10965-022-03326-6>
 38. Huang J, Yang H, Chen M, Ji T, Hou Z, Wu M (2017) An infrared spectroscopy study of PES PVP blend and PES-g-PVP copolymer. *Polym Test* 59:212–219
 39. Abdelrazek EM, Asnag GM, Oraby AH, Abdelghany AM, Alshehari AM, Gumaan MS (2020) Structural, optical, thermal, morphological and electrical studies of PEMA/PMMA blend filled with CoCl₂ and LiBr as mixed filler. *J Electron Mater* 49:6107–6122. <https://doi.org/10.1007/s11664-020-08342-0>
 40. Abdelrazek EM, Asnag GM, Oraby AH, Abdelghany AM, Alshehari AM (2020) Effect of addition of a mixed filler of CoCl₂ and LiBr into PEMA and its morphological, thermal and electrical properties. *Bull Mater Sci* 43:1–5. <https://doi.org/10.1007/s12034-020-02149-9>
 41. Mei GS, Menon PS, Hegde G (2020) ZnO for performance enhancement of surface plasmon resonance biosensor: a review. *Mater Res Exp* 7:012003. <https://doi.org/10.1088/2053-1591/ab66a7/meta>
 42. Farea MO, Abdelghany AM, Meikhaail MS, Oraby AH (2020) Effect of cesium bromide on the structural, optical, thermal and electrical properties of polyvinyl alcohol and polyethylene oxide. *J Mater Res Technol* 9:1530–1538
 43. Atta MM, Henaish AMA, Elbasiony AM, Taha EO, Dorgham AM (2022) Structural, optical, and thermal properties of PEO/PVP blend reinforced biochar. *Opt Mater* 127:112268
 44. Xu J, Liu Z, Wang J, Liu P, Ahmad M, Zhang Q, Zhang B (2022) Preparation of core-shell C@ TiO₂ composite microspheres with wrinkled morphology and its microwave absorption. *J Colloid Interface Sci* 607:1036–1049
 45. Sarkhel R, Ganguly P, Das P, Bhowal A, Sengupta S (2022) Synthesis of biodegradable PVA/cellulose polymer composites and their application in dye removal. *Environ Qual Manag.* <https://doi.org/10.1002/tqem.21920>

46. Abdelghany AM, Farea MO, Oraby AH (2021) Structural, optical, and electrical reinforcement of gamma-irradiated PEO/SA/Au NPs nanocomposite. *J Mater Sci Mater Electron* 32:6538–6549. <https://doi.org/10.1007/s10854-021-05371-1>
47. Yan J, Zou G, Wu A, Ren J, Hu A, Zhou YN (2012) Polymer-protected Cu-Ag mixed NPs for low-temperature bonding application. *J Electron Mater* 41:1886–1892. <https://doi.org/10.1007/s11664-012-2008-7>
48. Morsi MA, Pashameah RA, Sharma K, Alzahrani E, Farea MO, Al-Muntaser AA (2022) Hybrid MWCNTs/Ag nanofiller reinforced PVP/CMC blend-based polymer nanocomposites for multi-functional optoelectronic and nanodielectric applications. *J Polym Environ*. <https://doi.org/10.1007/s10924-022-02656-2>
49. Joshi JH, Kanchan DK, Joshi MJ, Jethva HO, Parikh KD (2017) Dielectric relaxation, complex impedance and modulus spectroscopic studies of mix phase rod like cobalt sulfide nanoparticles. *Mater Res Bull* 93:63–73
50. Rajeh A, Morsi MA, Elashmawi IS (2019) Enhancement of spectroscopic, thermal, electrical and morphological properties of polyethylene oxide/carboxymethyl cellulose blends: combined FT-IR/DFT. *Vacuum* 159:430–440
51. Al-Muntaser AA, Pashameah RA, Sharma K, Alzahrani E, Tarabiah AE (2022) Reinforcement of structural, optical, electrical, and dielectric characteristics of CMC/PVA based on GNP/ZnO hybrid nanofiller: nanocomposites materials for energy-storage applications. *Int J Energy Res* 46:23984–23995
52. Xia X, Zhong Z, Weng GJ (2017) Maxwell–Wagner–Sillars mechanism in the frequency dependence of electrical conductivity and dielectric permittivity of graphene-polymer nanocomposites. *Mech Compos Mater* 109:42–50
53. Ayesha AS (2008) Dielectric relaxation and thermal stability of polycarbonate doped with MnCl₂ salt. *J Thermoplast Compos Mater* 21:309–322. <https://doi.org/10.1177/0892705708089475>
54. Al-hakimi AN, Asnag GM, Alminderej F, Alhagri IA, Al-Hazmy SM, Abdallah EM (2022) Enhanced structural, optical, electrical properties and antibacterial activity of selenium nanoparticles loaded PVA/CMC blend for electrochemical batteries and food packaging applications. *Polym Test* 116:107794
55. Agrawal SL, Singh M, Asthana N, Dwivedi MM, Pandey K (2011) Dielectric and ion transport studies in [PVA: LiC₂H₃O₂]: Li₂Fe₅O₈ polymer nanocomposite electrolyte system. *Int J Polym Mater* 60:276–289. <https://doi.org/10.1080/00914037.2010.504178>
56. Atta A, Abdelhamied MM, Abdelreheem AM, Althubiti NA (2022) Effects of polyaniline and silver nanoparticles on the structural characteristics and electrical properties of methylcellulose polymeric films. *Inorg Chem Commun* 135:109085

Publisher's Note Springer Nature remains neutral with regard to jurisdictional claims in published maps and institutional affiliations.

Springer Nature or its licensor (e.g. a society or other partner) holds exclusive rights to this article under a publishing agreement with the author(s) or other rightsholder(s); author self-archiving of the accepted manuscript version of this article is solely governed by the terms of such publishing agreement and applicable law.